Supplementary Notes for
Using Synchronization for Prediction of High-Dimensional Chaotic Dynamics

Adam B. Cohen[1,2], Bhargava Ravoori[1,2], Thomas E. Murphy[1,3] and Rajarshi Roy[1,2,4]

[1]*Institute for Research in Electronic and Applied Physics, University of Maryland, College Park, Maryland 20742, USA*
[2]*Department of Physics, University of Maryland, College Park, Maryland, 20742 USA*
[3]*Department of Electrical and Computer Engineering, University of Maryland, College Park, Maryland 20742, USA*
[4]*Institute for Physical Sciences and Technology, University of Maryland, College Park, Maryland 20742, USA*
(Dated 12 September 2008)

I. Model and Numerical Computations

The simplest treatment of the optoelectronic feedback loop shown in Fig. 1 of the main manuscript models the low-pass and high-pass filters using first-order differential equations. This leads to the simple dynamical equations given in the main manuscript (Eq. 1) and published elsewhere. While this model can provide qualitative agreement with experimental observations [10], it is not sufficiently accurate for the synchronization method described here. In practice, the low-pass and high-pass filtering characteristics are determined by the bandwidth of the electronic amplifiers, which are not well described by a simple first-order response. To overcome this problem, we intentionally restricted the electrical bandwidth of the system by inserting a 7th order Butterworth low-pass filter with a cut-off frequency of 100 MHz cascaded with a 7th order Butterworth high-pass filter with a cut-on frequency of 1 MHz. The sharp roll-off characteristics of these filters ensures that the response is determined entirely by the passive filters rather than by the other electronic components in the loop. Moreover, the Butterworth filters have a known polynomial transfer function that can be easily incorporated into the numerical model. In general, an *n*th order linear time-invariant filter described by a rational transfer function may be represented by the state space differential equations [16]

$$\begin{aligned} \frac{d\mathbf{u}(t)}{dt} &= \mathbf{A}\ \mathbf{u}(t) + \mathbf{B}\ x_{in}(t) \\ x_{out}(t) &= \mathbf{C}\ \mathbf{u}(t) + D\ x_{in}(t) \end{aligned} \qquad \text{(S.Eq.1)}$$

where x_{in} and x_{out} are the scalar input and output respectively, $\mathbf{u}$ is an $n \times 1$ state vector, and $\mathbf{A}$, $\mathbf{B}$, $\mathbf{C}$, and D are matrices describing the filter. Because we used two cascaded 7th-order Butterworth filters (in effect, a 14th order band-pass filter), there are 14 first-order differential equations describing the filtering dynamics. Thus, $\mathbf{u}$ is a 14×1 vector, $\mathbf{A}$ is a 14×14 matrix, $\mathbf{B}$ is 14×1, $\mathbf{C}$ is 1×14, and D is a scalar number. The band-pass filters considered in our system are strictly proper, meaning their transmission falls to zero if the input frequency approaches

infinity. In this case, we require $D = 0$. The matrices **A**, **B**, **C**, and D can be calculated for any rational transfer function, or they can be directly synthesized for several classes of filters (e.g., Butterworth, Bessel, Chebyshev, etc.) using software such as MATLAB.

We may consider self-feedback as a relationship of the filter output to its input. In this case, the input to the filter is a nonlinear transform of the time-delayed output as

$$x_{in}(t) = -\beta \cos^2[x_{out}(t-\tau) + \phi_o] \qquad \text{(S.Eq.2)}$$

where τ represents the combined time-delay of the optical and electronic paths, ϕ_o is the bias point of the Mach-Zehnder modulator, and the negative sign appears because the photoreceivers used in our system incorporate an inverting amplifier stage. β, a dimensionless feedback strength proportional to the laser power P [μW], photoreceiver response R [V/μW], and amplifier gain G, is defined as

$$\beta = \frac{\pi GRP}{2V_\pi}. \qquad \text{(S.Eq.3)}$$

When defining the feedback strength β, we implicitly assume that the band-pass filter described above has unity gain for frequencies within the passband. All voltages are normalized to the Mach-Zehnder half-wave voltage V_π as

$$x(t) = \frac{\pi V(t)}{2V_\pi}. \qquad \text{(S.Eq.4)}$$

By substituting (S.Eq.2) into (S.Eq.1), one obtains the following nonlinear delay differential equation for the n-dimensional state space vector **u**:

$$\frac{d\mathbf{u}(t)}{dt} = \mathbf{A}\ \mathbf{u}(t) - \mathbf{B}\ \beta\ \cos^2\left[\mathbf{C}\ \mathbf{u}(t-\tau) + \phi_o\right] \qquad \text{(S.Eq.5)}$$

where we have assumed that $D = 0$, as appropriate for strictly-proper transfer functions. For the simple case when the band-pass filter is described by first-order low- and high-pass filters, the state space matrices can be realized as:

$$\mathbf{A} = \begin{bmatrix} -\left(\frac{1}{\tau_L} + \frac{1}{\tau_H}\right) & -\frac{1}{\tau_L} \\ \frac{1}{\tau_H} & 0 \end{bmatrix}, \quad \mathbf{B} = \begin{bmatrix} \frac{1}{\tau_L} \\ 0 \end{bmatrix}, \quad \mathbf{C} = \begin{bmatrix} 1 & 0 \end{bmatrix}, \quad D = 0. \qquad \text{(S.Eq.6)}$$

With this choice of matrices, (S.Eq.5) simplifies to the two coupled equations given in the manuscript (Eq.1). It is to be noted that in experiments, we observed only the single scalar variable $x(t)$ and not the internal variables pertaining to the filters described by the vector $\mathbf{u}(t)$.

In the experiments and simulations reported here, the Mach-Zehnder modulator was biased at the quadrature point, i.e., ϕ_o was set to $\pi/4$. The total round-trip time delay of the loop was measured to be 22.45 ns. We studied the dynamics as the feedback strength β is varied. Physically, this is related to varying the optical power P input to the modulator. Although (S.Eq.3) implies that β is proportional to P, in the experimental system the amplifier gain G is not flat over the entire spectral range from 1 – 100 MHz. Because the frequency content of the time series depends on the feedback strength, it is difficult to establish a simple linear relationship between β and P.

For simulations, the equations of motion were numerically integrated using Simulink, a graphical programming environment, and MATLAB. The integrations were performed using a fifth order Dormand-Prince method with a fixed step size of 0.005 ns.

II. Computation of Lyapunov Spectrum and Dimension

To compute the Lyapunov spectrum of the equations of motion (S.Eq.5), we employed the method put forth by Farmer [14]. Using matrices **A**, **B**, **C** and D that correspond to the cascaded 7th-order Butterworth high-pass and low-pass filters, one obtains a system of 13 coupled first-order ordinary differential equations and one first-order delay differential equation. In order to compute the Lyapunov spectrum, the time delay τ is divided into N discrete points. This allows one to replace the delay differential equation with a set of N ordinary differential equations, written in terms of the N variables evaluated at discrete points [18]. Together with the remaining equations, this yields N+13 first-order coupled ordinary differential equations. These

equations are linearized about a solution to yield the equations of motion for small perturbations. The linearized equations were solved with different initial condition vectors chosen to be orthogonal to each other. Each of these initial conditions signifies a perturbation along one direction in the associated (N+13)-dimensional phase space. The rates of growth of the magnitude of these initial condition vectors give the Lyapunov exponents in various directions. The Lyapunov exponents obtained by this method were averaged over a long time to obtain the global Lyapunov spectrum.

In our computations of the Lyapunov spectrum, we chose N = 113 (giving a time step of $dt = \tau / N \sim 0.2$ ns) and used a second order Heun's method to solve the differential equations.

Having the Lyapunov spectrum, the Lyapunov dimension can be computed using the Kaplan-Yorke conjecture

$$D_{KY} = M + \frac{\sum_{j=1}^{M} h_j}{\left| h_{M+1} \right|} \qquad \text{(S.Eq.7)}$$

where M is the largest number for which the sum of Lyapunov exponents $\sum_{j=1}^{M} h_j$ stays positive. Note that here the Lyapunov exponents are sorted in descending order.

III. Determining Maximum Lyapunov Exponent from a Time Series

The maximum Lyapunov exponent describes the exponential divergence rate between two initially close points in a phase space capturing the chaotic attractor. There exists a reliable method for determining the maximum Lyapunov exponent from a single time series using time-delay embedding techniques. The scheme involves finding nearby points in a d-dimensional time-delay embedding space and calculating the rate of separation as time progresses [18]. We report here a similar technique with one major difference: instead of searching through historical

data to find neighboring points in phase space, our data assimilation process entrains the simulation to produce a time series similar to the experimental time trace. This process may be viewed as forcing the simulation to a point nearby in multidimensional time-delay embedding space. Once the systems achieve a sufficient degree of synchrony, the predictor system is allowed to evolve independently and the rate of separation from the experimental trajectory yields the maximal Lyapunov exponent.

Supplementary Figure 1(a) shows the separation between the two traces on a semilogarithmic scale, as a function of time, evaluated for different choices of the embedding dimension d. In each case, the separation is calculated using a d-dimensional Euclidian norm, with an embedding time delay of 1 ns. Each successive trace is vertically offset for better differentiation. The exponential divergence rate is seen to be the same for all choices of d.

With an embedding dimension of $d = 1$, the Euclidean norm simplifies to the absolute difference $|x_1 - x_2|$, which goes to zero whenever the two one-dimensional time traces cross one another. This causes large apparent fluctuations in separation, when plotted on a semilogarithmic scale. As the d increases, these fluctuations are reduced because the likelihood of coincidental crossings is smaller in higher dimensional space.

An alternative technique to overcome this problem without using a multidimensional embedding is to apply a moving-window boxcar average to the 1-dimensional absolute difference. Supplementary Figure 1(b) compares the raw absolute difference to the smoothed difference, using a 25 ns moving boxcar average.

IV. Finite-Time Lyapunov Exponents

In this paper, we observe the exponential divergence between the predicted and measured time traces only over a finite time interval T. In practice, the length of time over which this

divergence can be observed depends on both the magnitude of the initial separation and the amplitude of the attractor. Because of these constraints, our method evaluates the finite-time Lyapunov exponent (FTLE), which can be regarded as a local measure of the divergence rate. In the limit that T goes to infinity, the finite-time Lyapunov exponent approaches the global maximum Lyapunov exponent, a measure that is independent of the starting point on the attractor.

By considering many different starting points on the attractor, one can construct a statistical distribution of finite-time Lyapunov exponents for the system [18]. The distribution of FTLEs for a chaotic attractor has been theoretically studied and can be approximated by a Gaussian distribution [13]. The mean of the Gaussian distribution is the global maximum Lyapunov exponent, and the distribution width σ is proportional to $1/\sqrt{T}$, where T is the finite time interval. Thus, as the time interval T is increased, the distribution of FTLEs narrows, eventually approaching a single global value. We have verified this effect using simulated time series data (Supplementary Figure 2).

For both the experimental and simulation probability distributions for prediction horizon times presented in the main manuscript (Figure 4(b)), each Lyapunov exponents was calculated by fitting over a finite-time interval T of 50 ns.

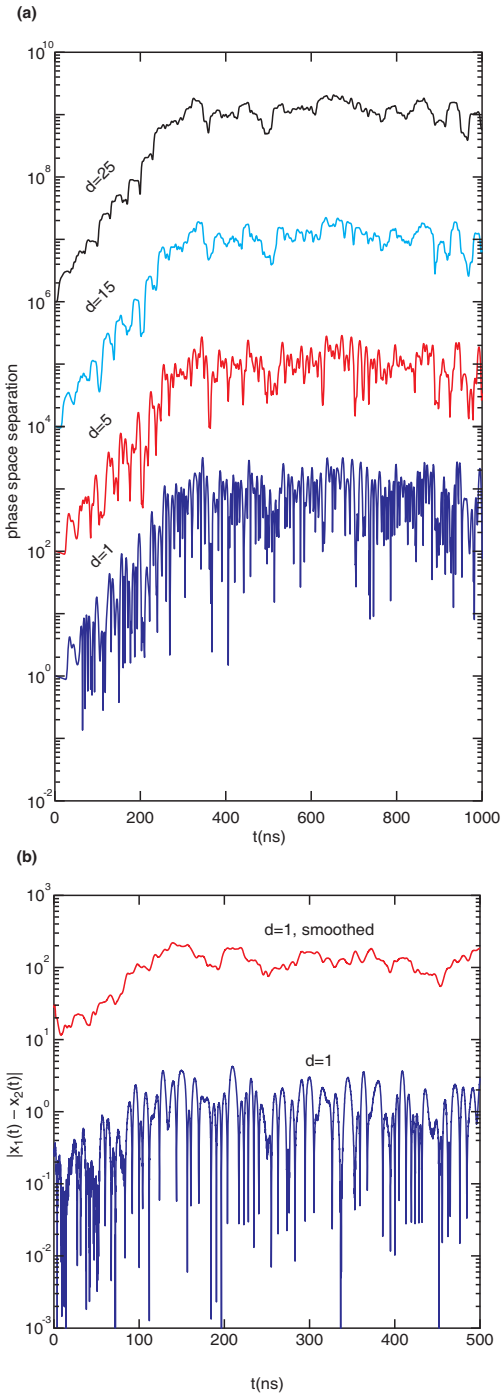

Supplementary Figure 1: Separation in an embedding phase space
(a) Semilogarithmic plot of phase space separation for varying embedding dimension with simulation data. The curves for d = 5, 15, 25 are raised artificially. (b) Semilogarithmic plot of absolute separation using experimental data. The upper curve is the same difference smoothed using a 25 ns moving window. The curve is artificially raised.

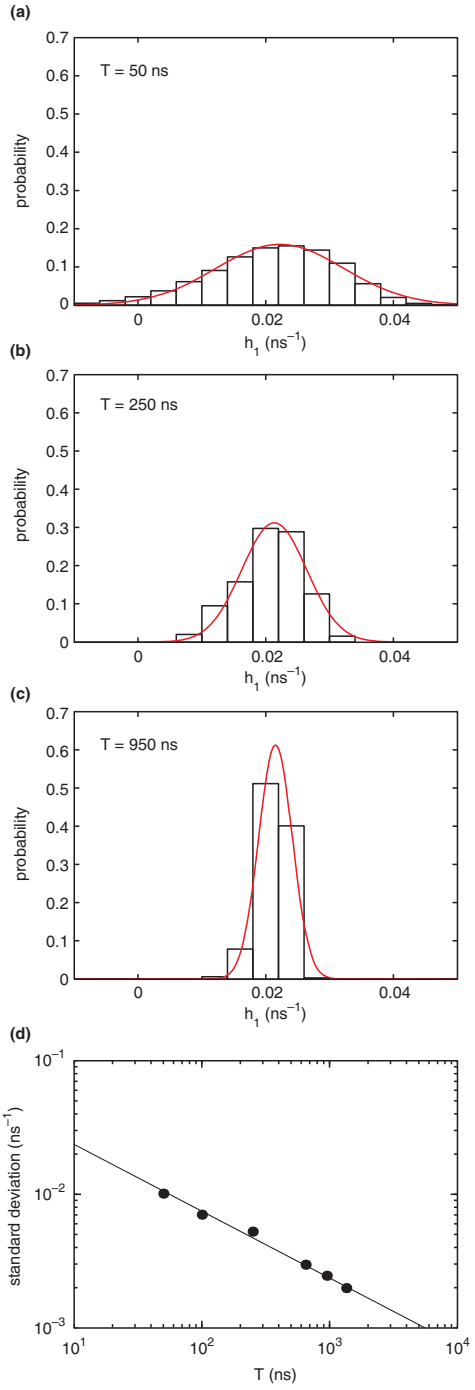

Supplementary Figure 2: Distribution of FTLEs
(a) – (c) shows three different distributions of finite-time Lyapunov exponents, calculated using finite time intervals of 50, 250 and 950 ns, respectively. As expected, the distribution of FTLEs becomes progressively narrower as the finite time interval is increased. (d) shows the standard deviation vs. the fitting time T, on logarithmic axes. The line with a slope of –1/2 shows the $1/\sqrt{T}$ dependence expected from theory.

Supplementary References

[16] C.T. Chen, *Linear System Theory and Design* (Oxford University Press, USA, 1998).

[17] J.-P. Eckmann, S.O. Kamphorst, D. Ruelle, and S. Ciliberto, Phys. Rev. A **34**, 4971 (1986).

[18] A. Prasad and R. Ramaswamy, Phys. Rev. E **60**, 2761 (1999).